Light-output enhancement of InGaN light emitting diodes regrown on nanoporous distributed Bragg reflector substrates

John C. Jarman, Tongtong Zhu*, Peter H. Griffin and Rachel A. Oliver

Department of Materials Science and Metallurgy, University of Cambridge, 27 Charles Babbage Road, Cambridge, CB3 0FS, United Kingdom. Email: tz234@cam.ac.uk

Utilising our novel wafer-scale electrochemical porosification approach which proceeds through the top surface by means of nanoscale vertical etching pathways, we have prepared full 2-inch wafers containing alternating solid GaN and nanoporous GaN (NP-GaN) layers that form distributed Bragg reflectors (DBRs), and have regrown InGaN-based light emitting diode (LED) heterostructures on these wafers. The NP-GaN DBR wafer is epi-ready and exhibits a peak reflectance of 95% at 420 nm prior to growth of the LED heterostructure. We observe a 1.8x enhancement in peak intensity of LED electroluminescence from processed devices, and delayed onset of efficiency droop with increased injection current.

1. Introduction

Gallium nitride (GaN) and its alloys with aluminium nitride and indium nitride form the basis for high-efficiency light-emitting diodes (LEDs) and laser diodes[1, 2], of widespread application in solid-state lighting[3]. The overall external efficiency of an LED may be influenced by a combination of the internal quantum efficiency of the multiple-quantum-well (MQW) structure, which depends on the rate of radiative compared to non-radiative carrier recombination; the current injection efficiency; and the efficiency with which photons may be extracted from the device (the light extraction efficiency, LEE)[4, 5]. This work focuses on a method for improving the LEE.

One method for optimising light extraction efficiency in InGaN LEDs is flip-chip technology, which detaches the entire LED structure from its native substrate, bonds the p-GaN layer to a conductive and reflective backplane, and roughens the n-GaN using an etch process to achieve a textured surface[5, 6]. However, such a process is complex and expensive, and is therefore limited to specialised high-brightness applications. Another popular technique for improving the LEE involves roughening or pre-texturing the sapphire substrate[7, 8], which also improves the quality of the subsequent GaN and LED epitaxy, and results in an overall increase in the light output by as much as 48%[9]. However, GaN growth on patterned sapphire substrates requires extra processing steps, and thus slows down LED production. More importantly, the light is scattered to a wider range of angles, and so efficiently controlling the direction of emitted light becomes more challenging.

Another strategy for increasing the extraction efficiency is the inclusion of distributed Bragg reflectors (DBRs) underneath the active layers of the device. A DBR consists of layers of alternating high and low refractive index material that can be defined during epitaxial wafer growth, and may therefore be inserted at a precise depth in the wafer, enabling application to devices such as resonant-cavity LEDs[10]. Alloys of AlGaN[11, 12] or AlInN[13, 14] may be used as the low-index material, with GaN or a different composition of AlGaN used as the high-index material. However, there will be a lattice mismatch between compositions of $Al_xGa_{1-x}N$ that will increase as the refractive index contrast increases, and this means that the achievable refractive index contrast is low. The number of layers is also limited by the strain build-up that can be tolerated without cracking, and this also restricts maximum reflectivity. AlInN, by contrast, may be lattice-matched to GaN, obviating strain-management issues; but its growth

is slow and refractive index contrast is still relatively low, making it an impractical option for low-cost devices.

Nanoporous GaN (NP-GaN)[15-17] is another option for use as the low-index material, with the resulting nanoporous DBRs (NP-DBRs) able to achieve high refractive index contrast and hence high reflectivity within a small number of layers. NP-GaN may be manufactured by a simple electrochemical or photoelectrochemical etch that is selective for the carrier density in the material, and is therefore controllable by including doped layers in the as-grown structure. As the growth only requires a variation in dopant concentration, rather than any adjustment of alloy composition, it is relatively fast and does not present issues relating to strain build-up in the material.

Several demonstrations of this concept exist in the literature; for example, Shiu *et al.* have demonstrated growth of a full LED structure, including p-i-n junction and MQWs, with a multilayer stack of alternating n-GaN and undoped-GaN layers grown underneath the LED. In that work, this latent DBR was porosified using electrochemical etching, with trenches patterned between devices to allow the etchant to access the buried doped layers and etch laterally[18]. Shieh *et al.* have also reported a similar method[19]. The inclusion of the NP-DBR underneath an LED device resulted in enhanced emission power in both electroluminescence (EL) and photoluminescence (PL) compared to a device without the NP-DBR in both cases. Similar results have been found for porous AlGaN DBRs[20] fabricated by similar methods underneath UV-emitting LEDs[21, 22]. However, such methods impose restrictions on the epitaxy of the device layers, as the doping levels must be selected so that the electrochemical etch does not porosify the LED heterostructure.

Regrowth of an LED heterostructure on top of a template containing NP-GaN is one possible solution to this issue. Regrowth of device layers on top of a thick NP-GaN layer has already been demonstrated[23], where the regrowth occurred after the electrochemical porosification process and a subsequent photoelectrochemical etch had been carried out. In addition to facilitating post-growth substrate removal, it was also noted that the presence of the porous layer also improved efficiency in the resulting devices – this was partly attributed to reduced strain and internal field across the MQWs, in addition to light reflection from the interface.

In this paper, we report a combination of these approaches; first creating an electrochemically etched NP-DBR structure in a GaN wafer, porosified without prior pattering through nanoscale

etching pathways, and then using this as a template for regrowth of an LED heterostructure. This method permits the use of established processes for growing high-efficiency LED structures, without the need to ensure compatibility with the electrochemical etch; and it also avoids the possibility of damage to the active layers during porosification. Our method also allows formation of the NP-DBR and growth of the LED to be optimised independently, allowing more freedom over doping levels present in the LED heterostructure as unintentional EC etching of the device layers is not a possibility.

2. Methods

GaN template growth and LED regrowth were carried out by metalorganic vapour phase epitaxy (MOVPE) on 2" c-plane sapphire substrates in a 6x2" close-coupled showerhead reactor from Thomas Swan. Trimethylgallium, trimethylindium, trimethylaluminium and ammonia were used as the Ga, In, Al and N sources, respectively. Silane and bis-(cyclopentadienyl)magnesium were used as the Si and Mg sources for n and p-doped material. Two templates were grown, with a low dislocation density of $3 - 6 \times 10^8$ cm^{-2}, and each containing a latent NP-DBR structure consisting of alternating layers of undoped and highly n-doped GaN.

The electrochemical porosification process, described in detail elsewhere[16], was then used to selectively porosify the highly-doped n-type layers in one of the templates. A 0.25 M solution of oxalic acid was used as the electrolyte, with indium solder used to contact the doped GaN layers. A positive bias of 6 V was applied between the sample and a platinum foil counter-electrode, injecting holes into the highly-doped n-type layers at the GaN/electrolyte interface. This selectively oxidises the gallium, which then dissolves and releases nitrogen. It is important to note here that no trenches were patterned into the GaN epitaxy prior to electrochemical etching. The etch can penetrate undoped GaN layers by means of nanoscale vertical pathways that exist in the as-grown material, and these allow each layer of the DBR to be etched sequentially until all the n-doped layers are fully porous. The etching process was run to completion, and the templates were then characterised by scanning electron microscopy (SEM) using a circular backscatter detector, and by atomic force microscopy (AFM) in tapping mode.

After porosification, the wafers were returned to the reactor for regrowth of n-doped GaN, 5 InGaN quantum wells (QWs) and a p-doped GaN/AlGaN superlattice to form the final p-i-n LED structure. Reflectivity spectra were measured from the as-grown template, the NP-DBR

template, and the final regrown LED wafer, using an Olympus BX51 microscope coupled to an Ocean Optics spectrometer and white-light source.

After regrowth, the devices were processed using photolithography and dry etching to define 600 nm deep isolation mesas, followed by photolithography, thermal evaporation and lift-off to define contacts. Ohmic contacts to n-GaN were achieved with a Ti/Al/Ti/Au multilayer, with layer thicknesses of 15/50/30/80 nm, annealed by rapid thermal annealing (RTA) at 710°C for 2 minutes in N_2. The p-GaN was contacted using a Ni/Au stack, with thickness 4.5/4.5 nm, that was also annealed by RTA in a mixture of equal parts N_2 and O_2 at 470°C for 5 minutes to form a transparent ohmic contact. Ti/Au pads (10/80 nm) were then defined on top of this layer to allow electrical connections to be made to the p-contact. The overall device structure is shown schematically in **Fig. 1**(a). Optical micrographs of the EL emission from both the non-porous (**Fig. 1**(b)) and porous (**Fig. 1**(c)) samples show reasonably uniform emission from both devices. This suggests that the growth of the LED layers is not significantly altered by the presence of a NP-DBR in the regrowth template.

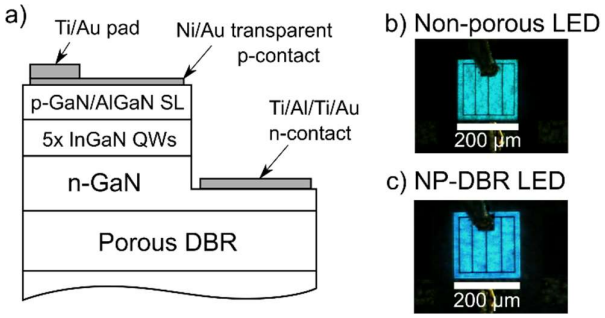

Fig. 1: (a) Schematic showing the structure of the processed wafers; optical micrographs of (b) non-porous and (c) NP-DBR devices.

Electrical and optical measurements were then conducted in a probe station, using an Ocean Optics USB2000+ spectrometer and silicon photodiode coupled to a 50x optical microscope by a 400 µm diameter optical fibre. A Keithley 2400 source-measure unit was used as a current and voltage source for L-I and I-V measurements respectively.

3. Results and discussion

Tapping-mode AFM images of the non-porous template (Fig. **2**(a)) show low rms roughness of 0.38 nm in a 5 x 5 µm region. Once the template has been subjected to EC etching to form the NP-DBR, the roughness remains almost unchanged at 0.40 nm (rms) (Fig. **2**(b)), indicating the suitability of the EC-etched template for regrowth.

SEM was performed with acceleration voltage of 5 kV to examine a cleaved cross-section of the porosified template. An image formed using the backscattered signal is shown in Fig. **2**(c), showing the formation of NP-GaN in layers which correspond to n-doped layers in the as-grown structure; the nanopores appear as dark dots lying in alternate layers of the structure, separated by regions of solid GaN. A large increase in the reflectivity of the sample, shown in Fig. **3**, is observed after the NP-DBR has been successfully porosified. Overgrowth of the LED structure is seen to cause a reduction to approximately 80% reflectivity from the peak of 95% observed from the NP-DBR template prior to regrowth.

Examination of the NP-DBR samples by SEM after regrowth (Fig. **2**(d)) reveals that some of the pores have become enlarged by the regrowth process, sometimes encroaching on the previously non-porous layers of the DBR. This effect appears to be most pronounced near the regrowth interface (at the top of the micrograph), suggesting that material is lost through the surface. The enlarged pores tend to be located in vertical stacks. Threading dislocations in the material have been suggested to act as vertical etching channels[16]; the same dislocations may allow material to evaporate from the sample when it is heated in the regrowth process, leading to vertically aligned regions of enlarged porosity.

The observed loss of material during regrowth will cause some degradation of the interface between the porous and non-porous layers, and will also reduce refractive index contrast, lowering NP-DBR reflectivity. The increased pore size will also contribute to increased scattering, also reducing the specular reflectivity of the DBR. This suggests there is room for further optimisation of the regrowth process to minimise the loss of material and hence maximise the reflectivity of the NP-DBR after the growth of device layers.

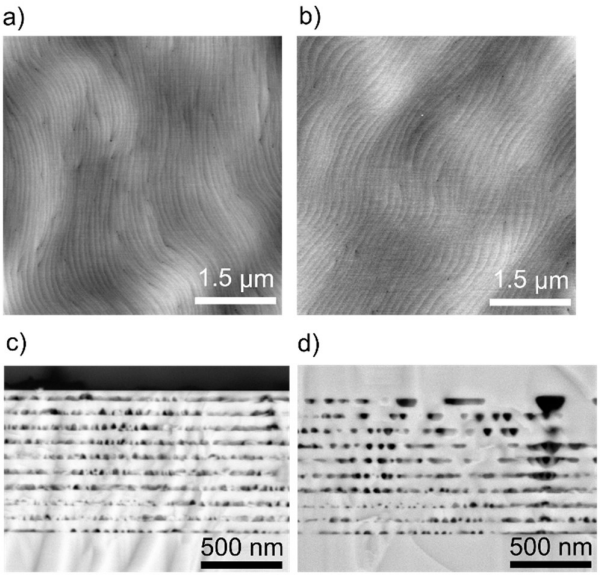

Fig. 2: AFM images of the template surface (a) before and (b) after EC porosification, showing a smooth surface and epi-ready terraces. Z-scale (black to white): 4 nm. Cross-sectional SEM images, taken using the backscattered electron signal, of nanoporous DBRs (c) before regrowth, and (d) after regrowth, showing enlargement of pores (dark contrast) and loss of material from the NP-DBR.

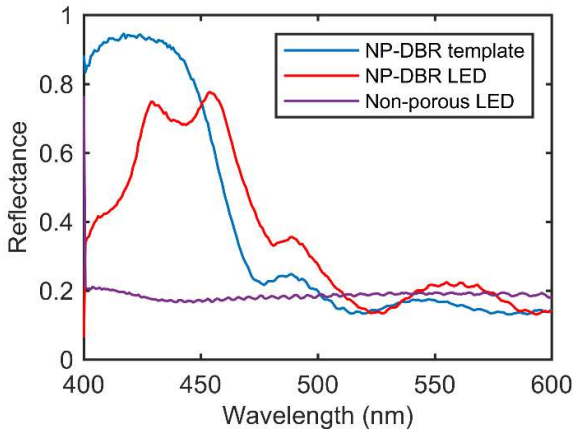

Fig. 3: Reflectivity spectrum measured from the NP-DBR template, compared with the reflectance of LED structures regrown on NP-DBR and non-porous templates.

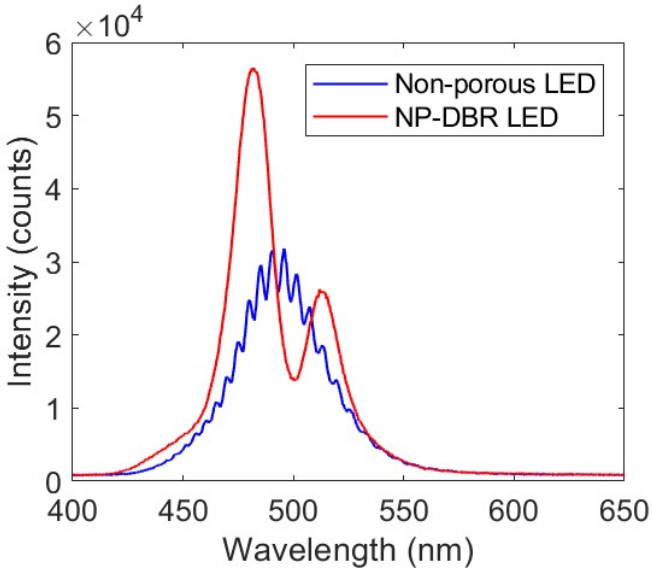

Fig. 4: Electroluminescence spectra from the two devices, obtained with a forward current of 20 mA, showing enhanced light output from the LED grown on a template containing a NP-DBR.

The electroluminescence (EL) emission spectra from the two devices, obtained with an forward current of 20 mA, are presented in Fig. **4**(d). Fabry-Pérot interference fringes can be observed in the spectrum obtained from the non-porous device, arising from reflections from the top and bottom interfaces of the GaN epilayer. The porosified wafer shows a sharper emission peak, with a clear dip associated with the cavity formed between the NP-DBR and top surface of the wafer at 500 nm. The peak intensity is also increased by a factor of 1.8, and the integrated intensity by a factor of 1.3.

The collection semi-angle for our EL setup is estimated to be 18°, and some of the enhancement we observe will be due to increased directionality of the LED. However, other studies that include angle-resolved measurements on LEDs incorporating NP-DBRs show that the divergence angle remains relatively high (80° for a NP-DBR LED compared to 120° for a standard LED)[19]. NP-GaN DBRs are also seen to have high diffuse reflectivity due to scattering that occurs in the porous structure[24], as well as retaining high specular reflectivity at large angles due to their high refractive index contrast. This suggests that the extraction efficiency, not just directionality, can be enhanced by such structures. The scattering effect of the NP-GaN may also help to extract light that would otherwise be trapped in laterally-propagating modes between the DBR and the surface of the wafer. Further study of the far-field emission pattern from these devices would help to address this question quantitatively.

The current-voltage (I-V) and light output-current (L-I) characteristics of the processed devices grown on porous and non-porous templates are compared in Fig. **5**, with the efficiency calculated as light output divided by injection current. The forward voltage at 20 mA was 3.0 V for the non-porous template, while a higher forward voltage of 3.8 V was measured for the device grown on the NP-DBR template. A higher series resistance is also observed in the NP-DBR device.

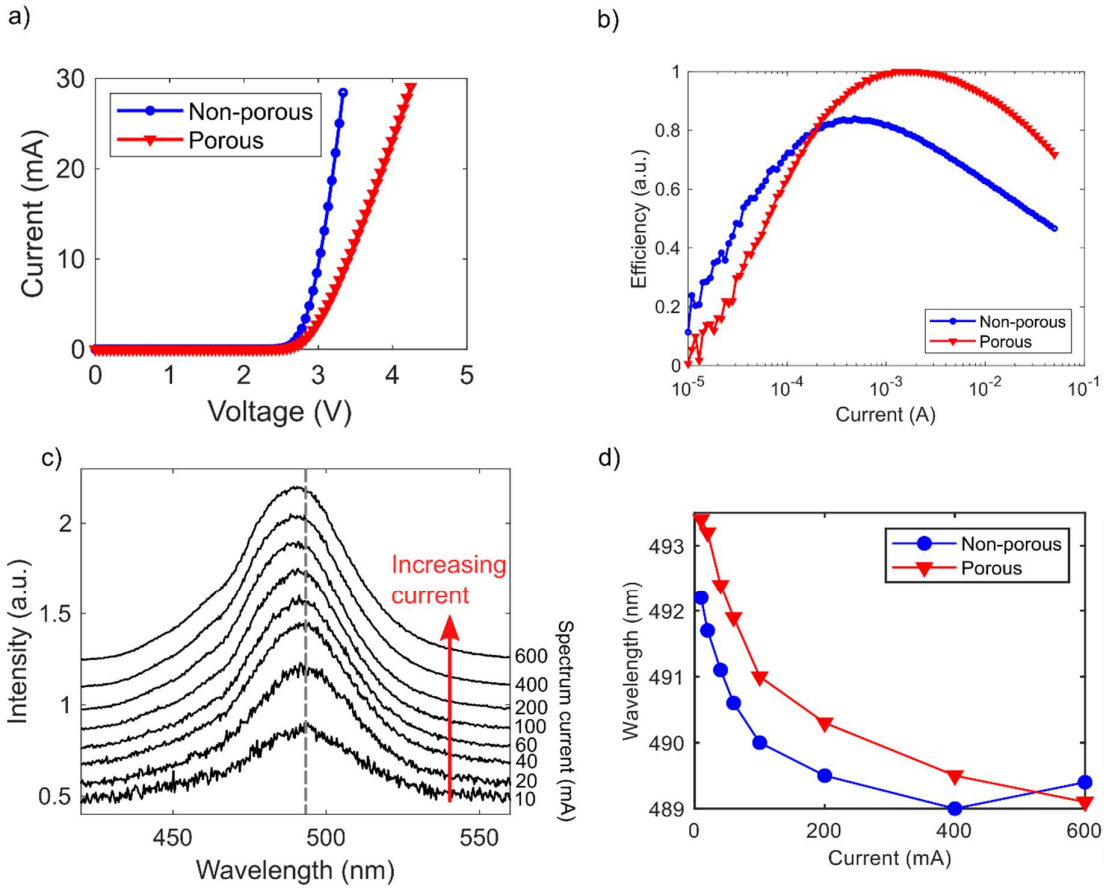

Fig. 5: (a) I-V and (b) L-I characteristics for the processed devices on porous and non-porous templates. (c) Spectra taken from NP-DBR LED, collecting side-emitted light, at increasing injection current. (d) Peak position for each device plotted as a function of current, showing similar blue-shift as injection current increases due to Coulomb screening of internal fields.

The onset of efficiency droop in the L-I plot was seen to occur at a higher current in the NP-DBR device. The L-I measurement was carried out under pulsed injection to limit thermal effects. There appears to be a lower efficiency in the porous device at low currents, which indicates a higher rate of defect-related non-radiative Shockley-Read-Hall (SRH) recombination[25]. The peak efficiency is also shifted to higher currents in the porous device. The change in the position of the efficiency peak could be an indication of modification of the electric fields across the QWs due to the presence of the porous layer, leading to shorter carrier

lifetimes[26, 27]. Such modification has been suggested to explain enhanced cathodoluminescence signals from LED structures overgrown on thick layers of porous GaN, where it was thought to be related to strain relief in the QWs[23]; strain relief will tend to lower the piezoelectric fields present across the heterostructure. Such a strain-relief effect has also been suggested to cause a blue-shift in the emission from LEDs on NP-DBRs compared to non-porous samples[18]. However, X-ray diffraction measurements provide no evidence for measurable relaxation in our samples.

Our investigation of the Stark shift in our samples also provided no evidence for modification of the electric fields in the QWs. We investigated this by changing the injection current in EL; increased carrier density in the QWs will act to screen any internal fields, resulting in a reduction in magnitude of the quantum-confined Stark shift, and a resulting blue-shift of the emitted light that depends on the magnitude of the pre-existing built-in fields[28]. To lessen the effect of heating on the samples, the spectra were taken approximately 1 ms after the current source was turned on, with an acquisition time of 10 ms. These spectra were also taken using light extracted from a cleaved edge of the wafer, to eliminate the cavity-related peak observed in the porous LED spectrum measured normal to the surface. This allows the underlying QW emission to be observed directly. The resulting measurements of the variation of emission wavelength with EL excitation power (Figure 4(d)) show a similar blue-shift in both porous and non-porous samples (which is in agreement with other similar studies of LED structures containing buried porous DBRs[18]), an observation which suggests that the internal fields are similar between the two samples. This suggests that the observed change in droop behaviour is not due to modification of the Stark shift in the QWs by the presence of the NP-DBR.

Another factor that affects droop performance of InGaN LEDs is the lateral current spreading behaviour, especially in the p-GaN layer. The local current density is not always uniform, with current density tending to crowd under the opaque, lower-resistance metallisation on top of the GaN mesa as current increases[29, 30]. The porous device will help to mitigate the losses caused by this current crowding, as some of the light ordinarily reflected from the p-GaN metallisation and lost in the substrate will instead be directed back towards the surface of the chip by the NP-DBR; this may help to delay the apparent onset of efficiency droop in such LEDs.

4. Conclusions

We have demonstrated the regrowth of a blue-emitting LED on a template containing an electrochemically-etched sub-surface NP-DBR. EL measurements indicate improvements to

the extraction efficiency from the devices and changes to the droop behaviour. The NP-DBR was formed using a vertical etching process, enabling the porosification of full wafers without requiring lithographically patterned trenches, and leaving the sample surface smooth and suitable for regrowth of device layers. Some degradation of the NP-GaN layers during regrowth was observed, suggesting that optimisation of the initial stage of the process could lead to further efficiency improvements.

Acknowledgements

This work was supported partly by the UK Engineering and Physical Sciences Research Council Grant No. EP/M011682/1 and the EPSRC Impact Acceleration Account Follow on Fund of the University of Cambridge. The authors would also like to thank Prof. Jeremy Baumberg and Alex Casalis de Pury for use of the instruments and assistance with the micro-reflectivity measurement.

Datasets for the figures in this paper can be found at https://doi.org/10.17863/CAM.37335.

References

1) S. Nakamura, T. Mukai and M. Senoh: Applied Physics Letters. **64** [13](1994)1687.

2) Y. Narukawa, J. Narita, T. Sakamoto, K. Deguchi, T. Yamada and T. Mukai: Japanese Journal of Applied Physics. **45** [10L](2006)L1084.

3) S. Pimputkar, J.S. Speck, S.P. DenBaars and S. Nakamura: Nature Photonics. **3** [4](2009)180.

4) Y.K. Ee, P. Kumnorkaew, R.A. Arif, H. Tong, J.F. Gilchrist and N. Tansu: Optics Express. **17** [16](2009)13747.

5) A. Laubsch, M. Sabathil, J. Baur, M. Peter and B. Hahn: IEEE Trans. Electron. Devices. **57** [1](2010)79.

6) T. Fujii, Y. Gao, R. Sharma, E. Hu, S. DenBaars and S. Nakamura: Applied Physics Letters. **84** [6](2004)855.

7) M. Yamada, T. Mitani, Y. Narukawa, S. Shioji, I. Niki, S. Sonobe, K. Deguchi, M. Sano and T. Mukai: Japanese Journal of Applied Physics. **41** [12B](2002)L1431.

8) Y.-J. Lee, J. Hwang, T. Hsu, M. Hsieh, M. Jou, B. Lee, T. Lu, H. Kuo and S. Wang: IEEE Photonics Technology Letters. **18** [10](2006)1152.

9) H.Y. Gao, F.W. Yan, Y. Zhang, J.M. Li, Y.P. Zeng and G.H. Wang: Journal of Applied Physics. **103** [1](2008)014314.

10) C. Zhang, K.L. Xiong, G. Yuan and J. Han: Physica Status Solidi a-Applications and Materials Science. **214** [8](2017)1600866. [in English].

11) N. Nakada, H. Ishikawa, T. Egawa, T. Jimbo and M. Umeno: Journal of Crystal Growth. **237** (2002)961.

12) K.E. Waldrip, J. Han, J.J. Figiel, H. Zhou, E. Makarona and A.V. Nurmikko: Applied Physics Letters. **78** [21](2001)3205.

13) E. Feltin, R. Butte, J.F. Carlin, J. Dorsaz, N. Grandjean and M. Ilegems: Electronics Letters. **41** [2](2005)94. [in English].

14) J.F. Carlin and M. Ilegems: Applied Physics Letters. **83** [4](2003)668.

15) C. Zhang, S.H. Park, D.T. Chen, D.W. Lin, W. Xiong, H.C. Kuo, C.F. Lin, H. Cao and J. Han: Acs Photonics. **2** [7](2015)980. [in English].

16) T. Zhu, Y.J. Liu, T. Ding, W.Y. Fu, J. Jarman, C.X. Ren, R.V. Kumar and R.A. Oliver: Scientific Reports. **7** (2017)45344. [in English].

17) S.-M. Lee, J.-H. Kang, J.K. Lee and S.-W. Ryu: Electron. Mater. Lett. **12** [5](2016)673.

18) G.Y. Shiu, K.T. Chen, F.H. Fan, K.P. Huang, W.J. Hsu, J.J. Dai, C.F. Lai and C.F. Lin: Scientific Reports. **6** (2016)29138.

19) B.C. Shieh, Y.C. Jhang, K.P. Huang, W.C. Huang, J.J. Dai, C.F. Lai and C.F. Lin: Applied Physics Express. **8** [8](2015)082101. [in English].

20) P. Griffin, T. Zhu and R. Oliver: Materials. **11** [9](2018)1487.

21) F.H. Fan, Z.Y. Syu, C.J. Wu, Z.J. Yang, B.S. Huang, G.J. Wang, Y.S. Lin, H. Chen, C.H. Kao and C.F. Lin: Scientific Reports. **7** (2017)4968. [in English].

22) G.J. Wang, B.S. Hong, Y.Y. Chen, Z.J. Yang, T.L. Tsai, Y.S. Lin and C.F. Lin: Applied Physics Express. **10** [12](2017)122102.

23) L.-W. Jang, D.-W. Jeon, A.Y. Polyakov, A.V. Govorkov, V.N. Sokolov, N.B. Smirnov, H.-S. Cho, J.-H. Yun, K.D. Shcherbatchev, J.-H. Baek and I.-H. Lee: Journal of Alloys and Compounds. **589** (2014)507.

24) J. Park, J.-H. Kang and S.-W. Ryu: Applied Physics Express. **6** [7](2013)072201.

25) J. Piprek: physica status solidi (a). **207** [10](2010)2217.

26) E. Sari, S. Nizamoglu, I.-H. Lee, J.-H. Baek and H.V. Demir: Applied Physics Letters. **94** [21](2009)211107.

27) A. David and M.J. Grundmann: Applied Physics Letters. **97** [3](2010)033501.

28) D.F. Feezell, J.S. Speck, S.P. DenBaars and S. Nakamura: J. Disp. Technol. **9** [4](2013)190.

29) B. Cao, S. Li, R. Hu, S. Zhou, Y. Sun, Z. Gan and S. Liu: Optics Express. **21** [21](2013)25381.

30) M.V. Bogdanov, K.A. Bulashevich, O.V. Khokhlev, I.Y. Evstratov, M.S. Ramm and S.Y. Karpov: Phys. Status Solidi C. **7** [7-8](2010)2124.

Figure Captions

Fig. 1: (a) Schematic showing the structure of the processed wafers; optical micrographs of (b) non-porous and (c) NP-DBR devices.

Fig. 2: AFM images of the template surface (a) before and (b) after EC porosification, showing a smooth surface and epi-ready terraces. Z-scale (black to white): 4 nm. Cross-sectional SEM images, taken using the backscattered electron signal, of nanoporous DBRs (c) before regrowth, and (d) after regrowth, showing enlargement of pores (dark contrast) and loss of material from the NP-DBR.

Fig. 3: Reflectivity spectrum measured from the NP-DBR template, compared with the reflectance of LED structures regrown on NP-DBR and non-porous templates.

Fig. 4: Electroluminescence spectra from the two devices, obtained with a forward current of 20 mA, showing enhanced light output from the LED grown on a template containing a NP-DBR.

Fig. 5: (a) I-V and (b) L-I characteristics for the processed devices on porous and non-porous templates. (c) Spectra taken from NP-DBR LED, collecting side-emitted light, at increasing injection current. (d) Peak position for each device plotted as a function of current, showing similar blue-shift as injection current increases due to Coulomb screening of internal fields.